Single cell transcriptomic profiling of neurodegeneration mediated by tau propagation in a novel 3D neuron-astrocyte coculture model

Hannah Rickner
Department of Biology, Boston University, Boston, MA, 02215
Lulu Jiang
Department of Pharmacology and Experimental Therapeutics, Boston University School of Medicine, Boston, MA, 02118 https://orcid.org/0000-0002-6918-6777
Rui Hong
Program in Bioinformatics, Boston University, Boston, MA, 02215
Nicholas K. O'Neill
Program in Bioinformatics, Boston University, Boston, MA, 02215
Benjamin Wolozin (bwolozin@bu.edu)
Department of Pharmacology and Experimental Therapeutics, Boston University School of Medicine, Boston, MA, 02118 https://orcid.org/0000-0003-2068-1475
Christine Cheng (chcheng@jcvi.org)
Department of Biology & Program in Bioinformatics, Boston University, Boston, MA, 02215; Informatics Group, J. Craig Venter Institute, La Jolla, CA, 92037

Letter

Keywords: Prion-like Process, Alzheimer's Disease, Neuron-astrocyte Spheroids, Toxic Tau Oligomers

Posted Date: March 1st, 2021

DOI: https://doi.org/10.21203/rs.3.rs-263918/v1

Version of Record: A version of this preprint was published at Alzheimer's & Dementia on December 1st, 2021. See the published version at https://doi.org/10.1002/alz.058551.

Abstract

Research into neurodegeneration has been hampered by lack of systems that accurately recapitulate neurodegenerative processes1. Propagation of tau through a 'prion-like' process has emerged as an important aspect of neurodegenerative diseases including Alzheimer's disease2. However, molecular mechanism of tau propagation is still largely unknown and a human 3D cellular model is still lacking. Here, we report development of the AstAD system, which uses human iPSCs to create neuron-astrocyte spheroids that incorporates propagation of toxic tau oligomers3,4. Single cell transcriptomic profiling reveals roles for ribosomes, TNF mediated neuroinflammation and heat shock proteins (HSP) as major elements of the disease stress response. Treatment with the HSP90 inhibitor PU-H71, which is selective for the dysfunctional HSP epichaperome, demonstrates reduction of pathology and neurodegeneration in the AstAD system5.

*Hannah Drew Rickner & Lulu Jiang contributed equally.

Main Text

Alzheimer's disease (AD) is characterized by the accumulation of misfolded, hyperphosphorylated tau which form neurofibrillary tangles and precipitates neurodegeneration. Neurodegeneration is initiated by multiple factors, including the accumulation of extracellular b-amyloid (Ab) plaques, inflammation and vascular dysfunction; these factors all converge on the neuron to produce tau pathology, which is most closely associated with cognitive decline[6]. The causes of AD are pleiotropic, but 95% of all cases are sporadic[7]. Current AD three-dimensional (3D) organoid models (mostly based on APP and presenilin mutations) do not show progressive tau aggregation beyond phosphorylated tau or develop neurodegeneration[1,8,9]. The difficulty in producing a human organoid model that exhibits tau pathology and neurodegeneration, combined with the inadequacies of current animal models for AD has stymied the field in its quest to understand the nature of sporadic AD and develop therapies able to delay AD disease progression.

We present a model, termed AstAD, that incorporates induced human neurons and astrocytes into a 3D organoid model, and then demonstrate induction of tau pathology with neurodegeneration by propagation using toxic tau conformers. Increasing evidence suggests that tau propagation is an important contributor to multiple human neurodegenerative diseases. Accumulating studies demonstrate that exogenous tau oligomers are internalized, trafficked, and propagated via release across cell junctions in animal and cell models, spreading disease pathology in a prion-like manner[2,10-18]. Most studies of tau propagation have focused on tau fibrils, which propagate pathology but elicit little if any neurodegeneration[2,10-18]. In contrast, we have shown that exposure to tau oligomers propagates tau pathology and induces robust neurodegeneration[3,19]. The AstAD system incorporates propagation of toxic tau oligomers to create a highly reproducible human 3D model of tauopathy. The AstAD system

enables analysis of neurodegenerative processes while also enabling concomitant analysis of the disease responses of astrocytes, which have recently been noted to play a large role in tauopathies[4,20-22].

To develop AstAD (diagramed in **Fig. 1A**) human iPSCs (hiPSCs) derived neural progenitor cells (NPCs) were directed into neuronal and astrocytic lineages. The neuronal lineage was created by NGN2 overexpression to produce hiPSC derived neuronal cell (hiNCs), while the astrocytic lineage was generated via small molecule-directed differentiation to produce hiPSC derived astrocytes (hiACs) (**Fig. 1A, Suppl. Fig. 1A**). The resulting hiNCs and hiACs were then combined into 3D culture termed asteroids (~2000 cells each) and allowed to develop over the course of three weeks (**Suppl. Fig. 1B-C**)[4]. Analysis of cell type markers showed robust differentiation of neurons that were positive for MAP2 and Tuj1 (**Fig. 1B, Suppl. Fig. 1D**) and astrocytes that were positive for S100β and GFAP (**Fig. 1B, E, Suppl. Fig. 1D**). Astrocytes incorporation was necessary for asteroid survival, and astrocytes exhibited processes that were striking for their length and complexity, as well as for the intimate association with developing neuronal processes (**Suppl. Fig. 1B, D, Suppl. Vid. 1**); the resulting highly arborized astrocytic morphologies resembled that observed *in vivo*.

Asteroid cellular phenotypes were also characterized by acquiring single cell RNA sequencing (scRNA-seq) profiles for 46,420 single cells with an average of 2000 genes per cell from varying experimental conditions across a time course of three weeks (**Suppl. Fig. 2**). Visualization by uniform manifold approximation and projection (UMAP) demonstrated the separation of cells into trajectory guided clusters (**Suppl. Fig. 3A**). These clusters were identified as the expected cycling neuronal progenitors (CYC), astrocytes precursors (ASC_P), astrocytes (ASC), and two subpopulations of neurons (NEU_A, NEU_B) based on the expression of established cell type specific genes including TOP2A and NES for cycling progenitors, SLC1A3, VIM, and CLU for astrocytes, and SNAP25, SYT1, MAP2, and STMN2 for neurons (**Suppl. Fig. 3A-C**). Manual cell typing was supported by the automated cell typing platform SingleR (**Suppl. Fig. 3D**). Notably, over 21 days of 3D co-culture (21 DIV3D) populations of cycling progenitor decreased while the populations of mature cell types increased (**Fig. 2B, D**).

We proceeded to model tauopathy in asteroid cultures. Oligomeric tau (oTau) was isolated from 9-month old PS19 P301S tau mice by centrifugation as described previously[3,23] (**Suppl. Fig. 4A**). hiNCs were exposed to oTau (0.04 mg/mL) for 24 hrs after which they were washed and combined with hiACs to generate the self-aggregating three-dimensional asteroid AD model (AstAD) (**Suppl. Fig. 4B**). Analysis of the AstAD cultures over 21 DIV3D showed rapid development of tau pathology, including tau hyperphosphorylation, misfolding, oligomerization and fibrilization (**Fig. 1**). Statistically significant increases in hyperphosphorylated tau were evident at positions S202/5 and S262 (**Suppl. Fig. 5C-H**). Misfolding and oligomerization of tau were observed using the MC1 and TOMA2 antibodies respectively, with each showing similar patterns of evolution (**Fig. 1B-D, Suppl. Fig. 5A-B)**. Fibrillar tau pathology also evolved, but at a slower rate. Fibrillar tau reactive with the dye thioflavine S became evident only at 21 DIV3D (**Fig. 1F, G**). The striking neuropathology was also associated with neurodegeneration by 21 DIV3D. Prominent neuronal injury was evident by 21 DIV3D with Fluoro Jade B (**Fig. 1 H-I**), reduced immunolabeling of MAP2 (**Suppl. Fig. 6A-B**) and increased LDH release (**Suppl. Fig. 6C**).

A requirement for oTau in the seeding process was demonstrated by immunodepleting oTau, which prevented any subsequent tau pathology or neurodegeneration (**Suppl. Fig. 4D**). The role of seeded oTau was further explored by exposing hiNCs to FITC labeled oTau. hiNC neurons exposed to FITC labeled oTau was present in >75% of hiNCs 24 hrs after seeding, however the vast majority of the seeded tau was degraded by 5 DIV3D (**Suppl. Fig. 4B-D**), and remaining FITC showing no correlation with accumulating tau pathology (**Suppl. Fig. 4D**). These results indicate that tau pathology developing after 5DIV3D must have been generated largely from endogenous tau sources.

Astrocytes also showed striking pathophysiological responses reminiscent of that observed in the human brain. The astrocytic markers S100β and GFAP showed statistically significant increases in reactivity beginning at 14 DIV3D and became prominent at the 21 DIV3D time point (**Fig. 1B, E, Suppl. Fig. 5E, I**). Astrocytic processes in the oTau AstAD cultures showed more intimate localization with neurons than in the control asteroid cultures (**Fig. 1B, Suppl. Vid. 1**). Taken together, these results indicate that over 21 DIV3D, the AstAD system develops a range of responses analogous to observed in the brains of human subjects with tau-mediated neurodegeneration.

A comparative analysis of control and AstAD scRNA-seq profiles across 21 DIV3D revealed shared and cell type specific transcriptional responses to oTau induced pathology (**Fig. 2A**). UMAP projections demonstrate changes in the relative proportion of cell types between control and AstAD over the course of growth in culture (**Fig.2B, D**). The neuronal cluster NEU_A (containing excitatory and inhibitory neuronal markers) and astrocytic cluster ASC increased in abundance, while the NEU_B cluster (containing only excitatory neuronal markers) decreased (**Fig. 2B, D**).

Differential gene expression analysis between the control and AstAD conditions within these clusters identified striking transcriptional changes over the time course. Notably, transcriptional changes were evident in both the ASC and NEU groups by 7 DIV3D, suggesting a high degree of interaction between the cell types (**Fig. 2C**). The AstAD system exhibited regulation of ribosomal transcripts, heat shock protein (HSP), chaperone transcripts, and TNF neuroinflammatory associated intermediate early response (IER) transcripts (**Fig. 2C, Suppl. Fig. 7**). Unexpectedly, an increase in ribosomal transcripts including RPS26 and RPS28 (green) dominated the early response at 7 DIV3D, suggesting a robust stress response (**Fig. 2C**). In contrast, suppression was observed for HSP (red) and TNF (purple) associated transcripts (**Fig. 2C**). This was reversed with increasing oTau pathology at 21 DIV3D, in parallel with increases in stress response transcripts including the TNF neuroinflammatory JUN, FOS, EGR1, and IER5 and HSP transcripts HSPA1B, DNAJB1, HSPB1, HSPH1, HSP90AB1, and HSP90AA1(**Fig. 2C**). By taking the average expression of all genes in a gene set for each cell we performed a comparative module analysis (see Methods) and demonstrated the observed transcriptional changes at 21 DIV3D in AstAD NEU_A align with transcripts upregulated in AD human brain[24,25], while AstAD ASC changes have a strong correlation with reactive astrocyte markers[26] and AD specific disease associated astrocytes[27] (**Fig. 2E**).

Functional enrichment analysis confirmed a strong ribosomal response at 7 DIV3D that weakened through 14 and 21 DIV3D (**Fig. 2F, H**). Pathways associated with neuron cell death, TNF

neuroinflammation, and HSPs were enriched among NEU_A upregulated genes at 21 DIV3D (**Fig. 2F, H**). While ASC shared the TNF pathway enrichment, they also demonstrated a more robust cytokine, HSP, and cell activation stress response suggestive of astrogliosis (**Fig. 2F, H**). Ontology module analysis highlights these responses in the TNFa via NFKB, transcription from RNA polymerase II promoter in response to stress, positive regulation of neuron death, and the HSP dominated response to topologically incorrect protein pathways at 21 DIV3D (**Fig. 2G, Suppl. Fig. 8**). Importantly, comparative functional enrichment reveals concordant responses between AstAD and single-nuclei transcriptomic profiles of postmortem AD brain, in particular the HSP response indicating activation of similar pathophysiological cascades[25,27,28] (**Suppl. Fig. 9**).

The inability of neurons to cope with accumulating tau pathology is hypothesized to stimulate formation of a dysfunctional epichaperome (high molecular weight complexes composed of HSP90 and HSP70 chaperones) and render neurons prone to degeneration[29]. The strong transcriptional response of HSPs in AstAD prompted us to test whether improving chaperone function by dispersing the dysfunctional epichaperome could delay disease progression. The AstAD cultures were treated with the epichaperome specific HSP90 inhibitor PU-H71 (1 μM, 3 days) that has been shown to disrupt the epichaperome complex (**Fig. 3A**)[5]. Subsequent analysis of pathology in AstAD showed a striking reduction in tau pathology and a corresponding reduction of neurodegeneration at 21 DIV3D (**Fig. 3**). We observed a significant reduction in tau phosphorylation (pS202/5, pS262), misfolding (MC1 antibody), oligomerization (TOMA2 antibody) and tangle formation (ThioS) (**Fig. 3B-E**). Fluoro Jade B reactivity also decreased, indicating a decrease in neuronal cell death (**Fig. 3G-H**). This reduction in neuronal stress and death was also accompanied by a decrease in astrogliosis, marked by decreased S100β and GFAP staining (**Fig. 3D, F**).

Analysis of the transcriptional responses by scRNA-seq supported the putative benefit observed for PU-H17, with the transcriptional profile shifting to that observed early in the disease process, perhaps prior to a point where the system was overwhelmed by oTau (**Fig. 4**). We observed a reduction in transcriptional changes associated with neuronal cell stress and death, including suppression of the TNF, HSP, neuron cell death, and transcriptional stress genes and modules (**Fig. 4B-E, Suppl. Fig. 8, 10**). Interestingly, PU-H71 initiated a striking re-expression of ribosomal transcripts at week 3 similar to that observed in week 1 in neurons (**Fig. 4B, D-E**). PU-H71 ablated the heat shock protein 70 response in astrocytes, perhaps indicating that the basal level of chaperones had become sufficient to cope with any oTau present (**Suppl. Fig. 10A**). These data suggest that dispersing the dysfunctional epichaperome was sufficient to reduce oTau induced neuropathology and neurodegeneration in AstAD.

We have presented a novel method for modeling tau pathology in a human iPSC derived co-culture of neurons and astrocytes in a rapid and reproducible manner. oTau seeding in hiNCs before combination with the hiACs allows for a specific analysis of how neuronal tau pathology interacts with surrounding astrocytes. This study provides the first single cell transcriptomic study of an organoid based tauopathy model. The astrocytic response to neuronal injury was surprisingly rapid and synchronized. Astrocytes and neurons both mounted robust ribosomal responses, consistent with an adaptation to stress.

Astrocytes were notable for mounting a more robust HSP response, perhaps contributing to their underlying resilience and enabling regulation of neuronal response[30,31]. Treatment with PU-H71 is known to disrupt the dysfunctional epichaperome, producing more functional molecular chaperones (HSP70 and HSP90)[5]. We saw a corresponding normalization of toxic TNF and neuronal death transcriptional signatures, as well as a reactivation of the ribosomal stress response, suggesting that this can be beneficial. It is notable that this was a short treatment with PU-H71, indicating that epichaperome inhibition could be a feasible option for treating the development of tauopathies at varying stages of progression.

References

1. Venkataraman, L., Fair, S.R., McElroy, C.A., Hester, M.E. & Fu, H. Modeling neurodegenerative diseases with cerebral organoids and other three-dimensional culture systems: focus on Alzheimer's disease. *Stem Cell Reviews and Reports* (2020).
2. Clavaguera, F., Grueninger, F. & Tolnay, M. Intercellular transfer of tau aggregates and spreading of tau pathology: Implications for therapeutic strategies. *Neuropharmacology* **76**, 9-15 (2014).
3. Jiang, L. *et al.* TIA1 regulates the generation and response to toxic tau oligomers. *Acta Neuropathol* **137**, 259-277 (2019).
4. Krencik, R. *et al.* Systematic Three-Dimensional Coculture Rapidly Recapitulates Interactions between Human Neurons and Astrocytes. *Stem cell reports* **9**, 1745-1753 (2017).
5. Inda, M.C. *et al.* The epichaperome is a mediator of toxic hippocampal stress and leads to protein connectivity-based dysfunction. *Nature Communications* **11**, 319 (2020).
6. Arriagada, P.V., Growdon, J.H., Hedley-Whyte, E.T. & Hyman, B.T. Neurofibrillary tangles but not senile plaques parallel duration and severity of Alzheimer's disease. *Neurology* **42**, 631-631 (1992).
7. Götz, J., Halliday, G. & Nisbet, R.M. Molecular Pathogenesis of the Tauopathies. *Annual Review of Pathology: Mechanisms of Disease* **14**, 239-261 (2019).
8. Choi, S.H., Kim, Y.H., Quinti, L., Tanzi, R.E. & Kim, D.Y. 3D culture models of Alzheimer's disease: a road map to a "cure-in-a-dish&quot. *Molecular neurodegeneration* **11**, 75-75 (2016).
9. Park, J. *et al.* A 3D human triculture system modeling neurodegeneration and neuroinflammation in Alzheimer's disease. *Nature Neuroscience* **21**, 941-951 (2018).
10. Wu, J.W. *et al.* Small misfolded Tau species are internalized via bulk endocytosis and anterogradely and retrogradely transported in neurons. *J Biol Chem* **288**, 1856-70 (2013).
11. Frost, B., Jacks, R.L. & Diamond, M.I. Propagation of tau misfolding from the outside to the inside of a cell. *J Biol Chem* **284**, 12845-52 (2009).
12. Guo, J.L. & Lee, V.M. Seeding of normal Tau by pathological Tau conformers drives pathogenesis of Alzheimer-like tangles. *J Biol Chem* **286**, 15317-31 (2011).
13. Guo, J.L. & Lee, V.M. Neurofibrillary tangle-like tau pathology induced by synthetic tau fibrils in primary neurons over-expressing mutant tau. *FEBS Lett* **587**, 717-23 (2013).

14. Clavaguera, F. *et al.* Transmission and spreading of tauopathy in transgenic mouse brain. *Nat Cell Biol* **11**, 909-13 (2009).
15. Lasagna-Reeves, C. *et al.* Alzheimer brain-derived Tau oligomers propagate pathology from endogenous Tau. *Scientific Reports* **2**(2012).
16. Clavaguera, F. *et al.* Brain homogenates from human tauopathies induce tau inclusions in mouse brain. *Proceedings of the National Academy of Sciences* **110**, 9535-9540 (2013).
17. Kfoury, N., Holmes, B.B., Jiang, H., Holtzman, D.M. & Diamond, M.I. Trans-cellular Propagation of Tau Aggregation by Fibrillar Species. *Journal of Biological Chemistry* **287**, 19440-19451 (2012).
18. Simón, D., García-García, E., Royo, F., Falcón-Pérez, J.M. & Avila, J. Proteostasis of tau. Tau overexpression results in its secretion via membrane vesicles. *FEBS Letters* **586**, 47-54 (2012).
19. Ashe, P.E.A. *et al.* TIA1 potentiates tau phase separation and promotes generation of toxic oligomeric tau. *PNAS* **(in press)**(2020).
20. Ben Haim, L., Carrillo-de Sauvage, M.-A., Ceyzériat, K. & Escartin, C. Elusive roles for reactive astrocytes in neurodegenerative diseases. *Frontiers in Cellular Neuroscience* **9**(2015).
21. Chun, H. & Lee, C.J. Reactive astrocytes in Alzheimer's disease: A double-edged sword. *Neurosci Res* **126**, 44-52 (2018).
22. Leyns, C.E.G. & Holtzman, D.M. Glial contributions to neurodegeneration in tauopathies. *Molecular Neurodegeneration* **12**, 50-50 (2017).
23. Apicco, D.J. *et al.* Reducing the RNA binding protein TIA1 protects against tau-mediated neurodegeneration in vivo. *Nat Neurosci* **21**, 72-80 (2018).
24. Blalock, E.M. *et al.* Incipient Alzheimer's disease: microarray correlation analyses reveal major transcriptional and tumor suppressor responses. *Proc Natl Acad Sci U S A* **101**, 2173-8 (2004).
25. Grubman, A. *et al.* A single-cell atlas of entorhinal cortex from individuals with Alzheimer's disease reveals cell-type-specific gene expression regulation. *Nature Neuroscience* **22**, 2087-2097 (2019).
26. Zamanian, J.L. *et al.* Genomic analysis of reactive astrogliosis. *The Journal of Neuroscience: The Official Journal of the Society for Neuroscience* **32**, 6391-6410 (2012).
27. Habib, N. *et al.* Disease-associated astrocytes in Alzheimer's disease and aging. *Nature Neuroscience* **23**, 701-706 (2020).
28. Mathys, H. *et al.* Single-cell transcriptomic analysis of Alzheimer's disease. *Nature* **570**, 332-337 (2019).
29. Inda, M.C. *et al.* The epichaperome is a mediator of toxic hippocampal stress and leads to protein connectivity-based dysfunction. *Nat Commun* **11**, 319 (2020).
30. Zhao, T., Hong, Y., Yin, P., Li, S. & Li, X.-J. Differential HspBP1 expression accounts for the greater vulnerability of neurons than astrocytes to misfolded proteins. *Proceedings of the National Academy of Sciences*, 201710549 (2017).
31. Taylor, A.R., Robinson, M.B., Gifondorwa, D.J., Tytell, M. & Milligan, C.E. Regulation of heat shock protein 70 release in astrocytes: role of signaling kinases. *Dev Neurobiol* **67**, 1815-29 (2007).

32. Dobin, A. *et al.* STAR: ultrafast universal RNA-seq aligner. *Bioinformatics* **29**, 15-21 (2013).
33. Butler, A., Hoffman, P., Smibert, P., Papalexi, E. & Satija, R. Integrating single-cell transcriptomic data across different conditions, technologies, and species. *Nat Biotechnol* **36**, 411-420 (2018).
34. Macosko, E.Z. *et al.* Highly Parallel Genome-wide Expression Profiling of Individual Cells Using Nanoliter Droplets. *Cell* **161**, 1202-1214 (2015).
35. McInnes, L., Healy, J. & Melville, J. UMAP: Uniform Manifold Approximation and Projection for Dimension Reduction. arXiv:1802.03426 (2018).
36. Benjamini, Y. & Hochberg, Y. Controlling the False Discovery Rate: A Practical and Powerful Approach to Multiple Testing. *Journal of the Royal Statistical Society. Series B (Methodological)* **57**, 289-300 (1995).
37. Wickham, H. *ggplot2: Elegant Graphics for Data Analysis*, (Springer Science & Business Media 2009).
38. Blighe K, R.S., Lewis M. EnhancedVolcano: Publication-ready volcano plots with enhanced colouring and labeling. R package version 1.8.0 edn (2020).
39. Raudvere, U. *et al.* g:Profiler: a web server for functional enrichment analysis and conversions of gene lists (2019 update). *Nucleic Acids Research* **47**, W191-W198 (2019).
40. Subramanian, A. *et al.* Gene set enrichment analysis: a knowledge-based approach for interpreting genome-wide expression profiles. *Proc Natl Acad Sci U S A* **102**, 15545-50 (2005).
41. Liberzon, A. *et al.* The Molecular Signatures Database (MSigDB) hallmark gene set collection. *Cell systems* **1**, 417-425 (2015).
42. Gu, Z., Eils, R. & Schlesner, M. Complex heatmaps reveal patterns and correlations in multidimensional genomic data. *Bioinformatics* **32**, 2847-9 (2016).
43. Merico, D., Isserlin, R., Stueker, O., Emili, A. & Bader, G.D. Enrichment map: a network-based method for gene-set enrichment visualization and interpretation. *PLoS One* **5**, e13984 (2010).
44. Shannon, P. *et al.* Cytoscape: a software environment for integrated models of biomolecular interaction networks. *Genome Res* **13**, 2498-504 (2003).

Materials And Methods

oTau Processing

Generation of S1p fraction: Frozen hippocampus and cortical tissues of 9-month old PS19 mice were weighed (100mg-250mg) and put in Beckman Centrifuge Tube, polycarbonate thick wall (cat # 362305). A 10 × volume of homogenization buffer was used to homogenize brain tissue with Hsaio TBS buffer (50 mM Tris, pH 8.0, 274 mM NaCl, 5 mM KCl) supplemented with protease and phosphatase inhibitor cocktails (Roche, cat#05892791001 and cat#04906837001), as described previously[3,23]. Briefly, the homogenate was centrifuged at 48,300 g for 20 min at 4 °C. The supernatant was then centrifuged a second time at 186,340 g at 4°C for 40 min. The TBS-extractable pellet (S1p) fraction was resuspended in

a 4x volume of TE buffer relative to the starting weight of the tissue homogenate, aliquoted and frozen at -80°C.

S1p fraction quantification:

Immuno-depletion of tau from S1p fraction: Tau aggregates in S1p fractions were eliminated from the fractions by a direct immuno-precipitation kit (Pierce, cat# 26148). Briefly, first tau-5 antibody was coupled to AminoLink plus Coupling Resin, and the fractions were pre-cleared using the Control Agarose Resin with all the materials provided by the kit. The sample was added to the antibody-coupled resin in the spin column and incubated in the column for overnight at 4°C on a gentle rotator. The column was centrifuged, and the flow-through saved for further experimentation. After 3 washes with IP buffer, the spin column was placed into a new collection tube, and tau plus antibodies were eluted from the resin. The eluate was analyzed for presence of tau.

Cell Culture and Treatment

All cell cultures were maintained at 37 °C with 5% CO_2. All cell counts were performed in quadruplicate using the Cellometer K2 with AOPI viability dye (Nexcelom).

Neural Progenitor Cell (NPC) Culture: Human iPSC (XCL-1) derived neural progenitor cells (NPCs, Stem Cell Tech 70901) were maintained in serum-free STEMdiff™ Neural Progenitor Medium 2 (Stem Cell Tech 08560) on Corning® Matrigel® hESC-qualified Matrix (Corning 354277) coated tissue culture plates. NPCs were plated at 50,000 cells/cm2 and passaged at 90% confluency by Accutase™ (Stem Cell Tech 07920) dissociation as necessary. A full media change was performed every other day. Low passage (passage <3) NPCs were cryopreserved in STEMdiff™ Neural Progenitor Medium 2 with 10% DMSO, and all NPCs used for experimentation were maintained at passage <6.

iPSC Neuronal Cell (hiNC) Differentiation: NPCs were passaged and plated at 50,000 cells/cm2 in STEMdiff™ Forebrain Neuron Differentiation Media (Stem Cell Tech 08600) on Corning® Matrigel® coated tissue culture treated plates and transduced with a NEUROG2 lentivirus (Genecopia LPP-T7381-Lv105-A00-S) at MOI 3 to induce iPSC derived neuronal cells (hiNC). After 24 hours of transduction, a full media change was performed.

iPSC Astrocytic Cell (hiAC) Differentiation: iPSC derived astrocytic cells (hiAC) were differentiated from NPCs by small molecule differentiation in STEMdiff™ Astrocyte Differentiation Media (Stem Cell Tech 100-0013) on Corning® Matrigel® coated tissue culture treated plates. A full media change was performed daily for four days, and cultures were passaged at 90% confluence by Accutase™. Cells were reseeded at 150,000 cell/cm2 and culture was continued in STEMdiff™ Astrocyte Differentiation Media with a full media change every other day for 14 days, passaging as necessary with Accutase™. At this stage the differentiated Astrocyte Precursor Cells (APCs) were cryopreserved in STEMdiff™ Astrocyte Differentiation Media with 10% DMSO. At time of use APCs were thawed and plated at 150,000 cell/cm2 in STEMdiff™ Astrocyte Maturation Media (Stem Cell Tech 100-0016) on Corning® Matrigel® coated

tissue culture treated plate. A full media change was performed every other day for 6 days, with one passage by Accutase™ at 90% confluence as necessary.

Asteroid Generation and Maintenance: A single cell suspension of hiNCs and hiACs was prepared by Accutase™ dissociation and washed once with DMEM/F12 (Stem Cell Tech 36254) to remove debris. hiNCs and hiACs were combined at a 1:1 ratio in Asteroid Media (DMEM/F12 (Stem Cell Tech 36254) , 1% Glutamax (Thermo Scientific 35050061), 1% Sodium Pyruvate (Thermo Scientific 11360070), 1% N-2 Supplement (Thermo Scientific 17502-048), 1% B-27 Supplement (Thermo Scientific 17504044), 10 uM Y-27632 (EMD Millipore SCM075) 1% PenStrep (Thermo Scientific 15140148), 1 mg/mL Heparin (Sigma-Aldrich H3149-250KU)) and plated in AggreWell™800 microwells (Stem Cell Tech 34815) coated with Anti-Adherence Rinsing Solution(Stem Cell Tech 07010). The AggreWell plate was immediately centrifuged at 100xg for 3 minutes to capture the cells in the microwells and incubated for 24 hours. A half media change was performed at 24 hours and then every other day for one week. At one week when the spheroids displayed a smooth, bright edge under the cell culture microscope cultures were transferred to ultra-low attachment round bottom 96 well plates (Fisher Scientific 07-201-680) and maintained in 100-200 uL asteroid media rotating at 85 rpm. A half media change was performed every other day for up to three weeks.

hiNC oTau Treatment: hiNCs were selectively exposed to 0.04 mg/mL oTau by direct administration in cell culture media for 24 hours before incorporation into asteroid culture.

PU-H71 Treatment: Asteroids were treated with 1 uM PU-H71 by direct administration in cell culture media for 72 hours before timepoint collection.

Sample Collection

Asteroid Fixation: At time of collection asteroids were transferred to a 1.5 mL Protein LoBind Eppendorf (Eppendorf 022-43-108-1) and allowed to settle. The supernatant was discarded and asteroids fixed in 4 °C 4% PFA in 1X PBS for 15 minutes, rotating at room temperature. After fixation, asteroids were washed 3x for 5 minutes each with 4°C 1X PBS, rotating at room temperature. Samples were stored in 1X PBS at 4 °C.

Conditioned Media Collection: 50 uL replicates of conditioned cell culture media from replicate asteroids were collected in flat bottomed 96 well plates and frozen at -20 °C.

Sample Processing

Immuno-fluorescence labeling: For immuno-labeling, selected asteroids from each condition were washed in 150µl PBS for 10 mins in the U-bottom 96-well plate and then permeabilized in 150µl PBS/0.01% Triton X-100 (PBST). The asteroids were then blocked in PBST supplemented with 5% BSA and 5% normal donkey serum for 1.5-2 hrs at room temperature (RT). After blocking, asteroids were incubated in primary antibodies dilute in 5% BSA/PBST and for overnight at 4°C. On the second day, the asteroids were

washed 3 times in PBST, 15 min each before they were transferring into 2° antibodies dilute (1:700 of Dylight-/Alexa-conjugated antibodies made in donkey purchased from Thermo Fisher Scientific in 5% BSA/PBST) for 2 hrs at RT. For DAPI nuclei stain, DAPI (1:10,000) was diluted in PBST and incubated with asteroids for 15 min followed by being washed 2x with PBST then 1x with PBS, 10 min each. The asteroids were then mounted onto microscope glass slides in Prolong gold antifade reagent. Primary antibodies used for asteroid labeling were as follows: Tuj1/beta3-Tubulin (chicken, SYSY, cat# 302 306, 1: 300), MAP-2 (rabbit, Millipore, cat# AB5622, 1: 1000), Rabbit monoclonal anti-S100β (Abcam, Cat# ab52642, 1:400); GFAP Monoclonal Antibody (Thermo Fisher Scientific, Cat#13-0300, 1:400); Mouse monoclonal anti-TOMA2 (provided by Dr. Rakez Kayed), 1:300; MC1 (provided by Dr. Peter Davies, Northwell), 1:300; CP-13 (provided by Peter Davies, Northwell), 1:300; AT-8 (provided by Dr. Nicholas Kanaan, Michigan State University), 1:300.

*Thioflavin S staining: T*he fresh made Thioflavin S (ThioS) solution was prepared by dissolving 1g of ThioS (Millipore Sigma, Cat# T1892) in 100ml 80% ethanol and was kept stirring for overnight at 4 °C before filtered for final use. The asteroids to be stained were washed sequentially in 70% and 80% ethanol, 1 min each, prior to incubating in ThioS/80% ethanol solution for 15 min. Asteroids were then sequentially washed in 80% and 70% ethanol, 1 min each, followed by two rinses in PBS. Asteroids were mounted in Prolong Gold antifade reagent and stored in the dark until imaging.

Flouro Jade B staining: The Flouro jade B reagent was purchased from EMD Millipore (Cat# AG310-30MG) and the staining protocol was followed as instructed by the manufacture. Briefly, the staining solution was prepared from a 0.01% stock solution for Fluoro-Jade B that was made by adding 10 mg of the dye powder to 100 mL of distilled water. To make up 100 mL of staining solution, 4 mL of the stock solution was added to 96 mL of 0.1% acetic acid vehicle. This results in a final dye concentration of 0.0004%. The stock solution, when stored in the refrigerator was stable for months, whereas the staining solution was typically prepared within 10 minutes of use and was not reused. Before staining, the asteroids were rinsed in distilled water and were then treated with 0.06% KMnO4 solution for 15 min. Then the asteroids were stained with FluoroJade B working solution for 30 min followed by being washed with PBS 5 min twice. Asteroids were mounted in Prolong Gold antifade reagent and stored in the dark until imaging.

LDH Cytotoxicity Assay: The CytoTox 96 Non-Radioactive Cytotoxicity Assay was performed as per manufacturer's instructions using 50 uL conditioned media replicates to measure lactate dehydrogenase (LDH) release (Promega G1780). Absorbance readings at 490 nm were taken on a SpectraMaxM5plate reader with SoftMax Pro 7.1 software.

Single Cell RNA Sequencing Sample Preparation and Sequencing: 30 asteroid per condition were pooled in a 1.5 mL Protein LoBind Eppendorf (Eppendorf 022-43-108-1) and allowed to settle. The supernatant was carefully discarded and a single cell suspension was produced by incubation in 500 uL digestion buffer (Accutase™ with 80 U/mL Protector RNase Inhibitor (Sigma-Aldrich 03335402001)) for 1 hour at 37 °C with gentle pipette mixing every 10 minutes. At the end of the incubation the single cell suspension

was washed with 500 uL wash buffer (0.02% BSA in 1X PBS with 80 U/mL Protector RNase Inhibitor) and passed through a 20 uM filter (MACS, Miltenyi Biotec 130-101-812) to a fresh 2 mL Protein LoBind Eppendorf. An additional 1 mL of wash buffer was then passed through the same filter for a total single cell suspension of 2 mL. The samples were centrifuged at 300 g for 5 minutes at 4 °C followed by another was in 1 mL wash buffer. After another centrifugation the supernatant was discarded and the single cell pellet gently resuspended in 50 uL wash buffer. Cells were counted in quadruplicate on the Cellometer K2 with AOPI and processed through the single cell RNA-sequencing pipeline from 10X Genomics, 3' Version 3 (10X Genomic Chromium).

Briefly, the single cell suspension was mixed with RT reaction mix to target a 8000 cell recovery and 75 ul was loaded onto a chromium microfluidics chip with 40 µL of barcoded beads and 280 µL of partitioning oil. The chip was run on the chromium controller, encapsulating a single cell and barcoded bead within individual oil droplets. Reverse transcription was performed within these individual oil droplets to produce barcoded cDNA. cDNA was then isolated by Silane DynaBeads (Thermo Fisher Scientific, Dynabeads MyONE Silane, Cat# 37002D) before PCR amplification. Amplified cDNA cleanup and size selection was performed using SPRIselect beads (Beckman-Coulter, SPRIselect, Cat# B23317) and cDNA quality was assessed by the High-Sensitivity DNA assay (on the Agilent 2100 BioAnalyzer (Agilent, High-Sensitivity DNA Kit, Cat# 5067-4626). Sequencing libraries were then prepared according to 10X specification, including fragmentation, sequencing adaptor ligation, and sample index PCR. Between each of these steps, library cleanup and size selection was performed by SPRIselect beads. Final cDNA library quality was assessed by the Agilent BioAnalyzer High-Sensitivity DNA assay and the Qubit High-Sensitivity DNA assay and quality-confirmed libraries were sequenced on Illumina's NextSeq 500 platform to a depth of 200 million paired-end reads.

Data Analysis

Images Analysis: Images were captured by Carl Zeiss confocal LSM700. The immuno-fluorescence stained DAPI-positive cells in each image of asteroids were quantified by Image J with function of automatically cell counting. The staining intensity in immuno-fluorescence labeled asteroids were measured by ImageJ. The intensity of MC1, TOMA2, CP13, AT8, ThioS and Fluoro-jade B were normalized by DAPI numbers. Schematics were created with BioRender.com.

*GraphPad Prism Statistical analysis :*Statistical analyses and figures artwork were performed using GraphPad Prism version 9.00 for Windows with two sided α of 0.05. All group data are expressed as mean ± SEM. Colum means were compared using one-way ANOVA with treatment as the independent variable. And group means were compared using two-way ANOVA with factors on oTau treatment and time points, respectively. When ANOVA showed a significant difference, pair wise comparisons between group means were examined by Tukey's, Dunnett or uncorrected Fisher's LSD multiple comparison test. Significance was defined when $p < 0.05$. LDH assay data analysis was performed in with a paired t-test.

Single Cell RNA Sequencing Data Analysis

CellRanger Pipeline: CellRanger version 3.1.0 (10X Genomics) was used to combine and process the raw Illumina NextSeq 500 RNA sequencing data. First each sequencing library was demultiplexed by sample index to generate FASTQ files for paired-end reads using the CellRanger mkfastq pipeline. FASTQ files were then passed to the CellRanger count pipeline, which used STAR aligner[32] to align reads to the human reference genome (GRCh38). The CellRanger aggr pipeline was then used to equalize the aligned molecule_info.h5 sample libraries across sequencing depths (by each sample cell being down-sampled to have the same confidently mapped reads per cell) and aggregated together to generate the gene-cell barcode matrix.

Seurat Object Filtration: Subsequent filtering, normalization, and scaling of data was performed using Seurat version 3.2.2 [33,34]. The Seurat object was created with a min.cells of 3 and a min.features of 200. Cells with less than 200 and greater than 5000 detected genes or greater than 20% mitochondrial counts were filtered out. Samples were subset to a max.cells.per.ident of 4642. Gene counts for each cell were normalized by total expression, multiplied by a scale factor of 10,000 and transformed to log scale. PCA based on the highly variable genes detected (dispersion of 2) was performed for dimension reduction and the top 20 principal components (PCs) were selected. We clustered cells based on graph-based methods (KNN and Louvain community detection method) implemented in Seurat. Clusters were visualized using uniform manifold approximation and projection (UMAP)[35] .

Cluster Cell Type Identification: To identify neuronal cell type subpopulations, we performed differential expression analysis using the Wilcoxon rank-sum test implemented in Seurat between previously defined clusters with a min.pct or 0.1, logfc.threshold of 0.25, and a pseudocount of 1E4 . This identified top expressing genes for each cluster, which were then considered alongside the feature expression of canonical gene cell type markers to conclude cell type cluster identification.

DE analysis: Differential expression analysis was performed for each cell type between control and AstAD samples using the Wilcoxon rank-sum test implemented in Seurat with a min.pct of 0.1, a logfc.threshold of 0.1, and a pseudocount of 1E4. A multiple comparison correction was performed using the Benjamin & Hochberg FDR method to produce an adjusted p-value [36]. Differentially expressed genes were evaluated according to their log fold change (greater than log2(.25)) and adjusted *p* values (0.05). All figures were generated using the ggplot2 R package and associated EnhancedVolcano R package [37,38].

Functional enrichment analysis: Functional geneset enrichment analysis of the significant differential genes between control and AstAD samples was performed using the R implemented GProfiler2 [39]. The enrichment analysis was run as an ordered query (ordered by log2FC) using a threshold of 0.05 and using Benjamin & Hochberg FDR for multiple testing correction[36]. Only genes in the Seurat dataset were considered by using a custom domain scope. A custom source GMT, gp__zSEF_sD9Q_d1M, was used. It includes all Hallmark gene sets, curated gene sets, and ontology gene sets from the Molecular Signatures Database (MsigDB) v7.2 [40,41]. The enrichment analysis was assessed and visualized by a heatmap of significance (−log10(*p* value)) of the top 20 enriched pathways per sample comparison. Comparative functional geneset enrichment analysis between AstAD and published datasets was performed with the

same gprofiler2 settings, but as a non-ordered query. Gene input was as follows: From AstAD dataset, genes upregulated in NEU_A, NEU_B, and ASC at 21 DIV3D (n=129, p <0.05, log fold change > 0.25). From Grubman et al. 2020[25] genes upregulated in AD DEG 5 and 7 (n = 109, log fold change > 1 and FDR < 0.01).From Mathys et al. 2020[28] , genes upregulated in late-pathology cases that are common to ≥5 cell types (n=16, log fold change > 1 and FDR < 0.01)). The enrichment analysis was assessed and visualized by a heatmap of significance (−log10(*p* value)) of the top 10 enriched pathways per data set. All heatmaps were generated using the ComplexHeatmap R package and color scale generated using dependent R package circilize[42]. Additional visualization of significant (p< 0.01) enriched pathways was performed using Cytoscape EnrichmentMap[43,44] with an edge cutoff of 0.375. Gene sets in EnrichmentMap cluster by similarity, and annotates of shared gene set features were added manually using Cytoscape implemented AutoAnnotate.

Module analysis: The scaled expression per cell of literature curated and MsigDB ontology genesets (see Source Table 1. Genesets) was compared between control and AstAD samples by computing the mean expression using colMeans and performing a t.test across comparison pairs using stat_compare_means. Figures were generated using the ggplot2 R package[37].

Data Availability: Raw and processed scRNA-seq data are available from GEO under accession GSE165587. Processed scRNA-seq datasets are available on Single Cell Portal, including the cell barcodes, UMAP coordinates, and other available characteristics. The processed scRNA-seq data is available at https://singlecell.broadinstitute.org/single_cell/study/SCP1271/asteroid1. The source data underlying Fig. 2, 4 and Suppl. Fig. 4C, 7-10 are provided in the Source Data files as follows: Source data of differential gene expression and celltype_markers is available in supplemental file asteroid1_sourcefile_deg and source data of gprofiler2 functional geneset enrichment, Source Table 1, Source Table 2, and Source Table 3 are available in supplemental file asteroid1_sourcefile_gpro.

Code Availability: The original R scripts for Seurat processing are available on github [https://github.com/satijalab/seurat). All custom code to reproduce the analyses and figures reported in this paper are available on github (https://github.com/ChristineLab/asteroid1).

Declarations

Author Contributions

H.D.R. designed and performed the experiments and bio-informatics analysis, interpreted the results, and wrote the paper. L.J. designed, performed and analyzed the experiments, interpreted the results, and wrote the paper. R.H. helped design statistical tests for scRNA-seq analysis. N.K.O'N. helped design statistical tests for scRNA-seq analysis. B.W. conceived and oversaw the project, provided guidance, interpreted the results and wrote the paper. C.S.C. conceived and oversaw the project, provided guidance, interpreted the results and wrote the paper.

Acknowledgements

We thank Dr. Todd A. Blute for his technical support at BU's Proteomics and Imaging Core Facility. We thank Rakez Kayed (UT Galveston) for provision of the TOMA2 antibody, Nicholas M. Kanaan (Michigan State University) for provision of the Tau13 antibody (originally created by Lester I Binder, Northwestern University), and Peter Davies (Northwell/Hofstra, deceased) for provision of CP13 antibody. We would like to thank the following funding agencies for their support: B.W. & C.S.C : Kilachand Fund of the BU Center for Life Sciences Engineering, B.W.: NIH (AG050471, AG056318, AG064932, AG061706) and the BrightFocus Foundation, C.S.C: NIH (DA047032, DA051411, DA051889, DA050243).

Additional Information/Competing Interests Statement

The authors declare the following competing interests:

B.W. is co-founder and Chief Scientific Officer for Aquinnah Pharmaceuticals Inc.

B.W., C.S.C, L.J, and H.D.R are submitting a patent application through Boston University entitled "Modeling Alzheimer's disease using 3D iPSC cultures."

Figures

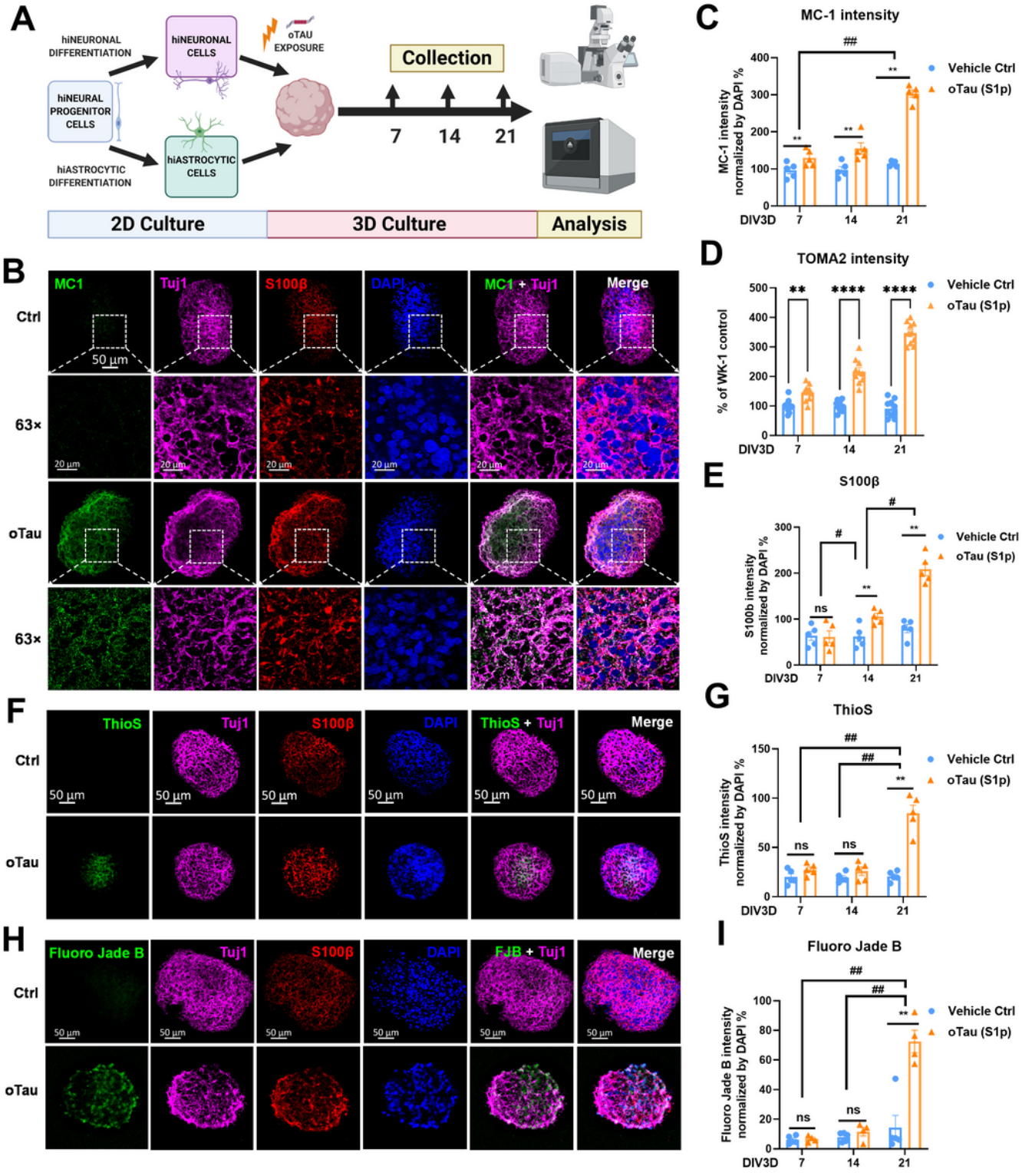

Figure 1

oTau seeding induces rapid accumulation of toxic tau and neurodegenerative pathology in the 3D neuron and astrocyte co-culture AstAD model. A. Experimental schematic including 2D culture, 3D culture, and analysis with indicated data collection timepoints. B. Representative images showing tau misfolding in oTau seeded asteroids at 21 DIV3D. The misfolded tau is labeled by MC1 (misfolded tau, green). Neurons were labeled by Tuj1 (βIII tubulin, violet) and astrocyte were labeled by S100β (Red). The bottom row

shows high magnification of the highlighted regions for the oTau panels. Scale bars: 10 μm and 50μm. C. Quantification of MC1 labeled fluorescence intensity normalized to the corresponding DAPI intensity. Data obtained from 5 independent asteroids. Error bars = SEM. Two-way ANOVA with Tukey's multiple comparisons test was performed, **p<0.01 comparisons to Vehicle control at each time point. ##p< 0.01 comparison to 7 DIV3D. D. Quantification of oligomeric tau by fluorescence intensity of TOMA2, normalized to the corresponding DAPI intensity. Data was from 10 independent asteroids. Error bars = SEM. Two-way ANOVA with Tukey's multiple comparisons test was performed, **p<0.01, ****p<0.001 comparisons to vehicle control at each time point. E. Quantification of astrocytic S100β labeled fluorescence intensity, normalized to the corresponding DAPI intensity. Data was collected from 5 independent asteroids. Error bars = SEM. Two-way ANOVA with Tukey's multiple comparisons test was performed, **p<0.01 comparisons to Vehicle control at each time point. ##p< 0.01 comparison to 7 DIV3D. F. Representative images showing Thioflavine S (ThioS) labeling at 21 DIV3D. Neurons were labeled by Tuj1 (βIII tubulin, violet) and astrocyte were labeled by S100β (Red). The bottom row shows high magnification of the highlighted regions for the oTau panels. Scale bars: 50μm. G. Quantification of ThioS labeled fluorescence intensity normalized to corresponding DAPI intensity. Data obtained from 5 independent asteroids. Error bars = SEM. Two-way ANOVA with Tukey's multiple comparisons test was performed, **p<0.01 comparisons to Vehicle control at each time point. ##p< 0.01 comparison to 7 DIV3D. H. Representative images quantifying neurodegeneration with Fluoro Jade Blue labeling at 21 DIV3D. Neurons were labeled with Tuj1 (βIII tubulin, violet) and astrocyte were labeled with S100β (Red). The bottom row shows high magnification of the highlighted regions for the oTau panels. Scale bars: 50μm. I. Quantification of Fluoro Jade Blue labeled fluorescence intensity normalized by corresponding DAPI intensity. Data obtained from 5 independent asteroids. Error bars = SEM. Two-way ANOVA with Tukey's multiple comparisons test was performed, **p<0.01 comparisons to Vehicle control at each time point. ##p< 0.01 comparison to 7 DIV3D.

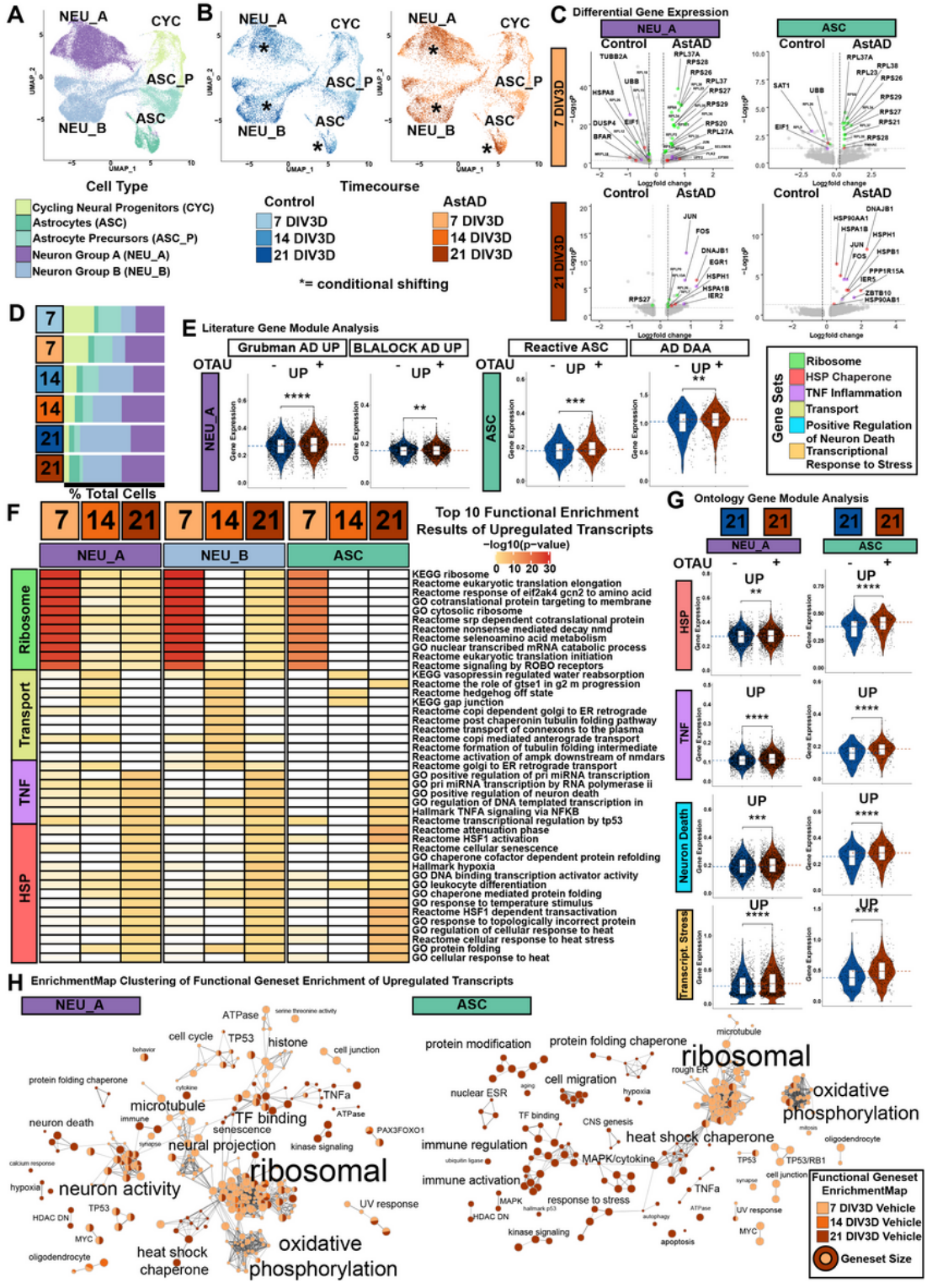

Figure 2

Single cell RNA-sequencing of AstAD reveals dynamic transcriptional response to oTau induced pathology. A. Uniform Manifold Approximation and Projection (UMAP) of 44,701 cells from all experimental conditions after filtration and cell type identification (see Methods). Five cell types are identified, neuron group A (NEU_A, purple), neuron group B (NEU_B, blue), astrocytes (ASC, green), astrocyte precursors (ASC_P, teal) and cycling neuronal progenitors (CYC, yellow). B. UMAP colored by

experimental conditions across the 21 DIV3D control and AstAD time course (blue and orange gradient, respectively) highlighting model trajectory. Asterisks indicate regions of conditional shifting between control and AstAD. C. Differential gene expression between control and AstAD at 7 DIV3D and 21 DIV3D presented as volcano plots. Dotted lines indicate a log 2 fold change significance of magnitude 0.25 and a p-value significance of 0.05. Significant differentially expressed ribosomal genes are highlighted in green, HSP associated genes are highlighted in red, and TNF inflammatory genes are highlighted in purple. D. Percent composition of cell type clusters within each condition across the 21 DIV3D time course out of 100% total cells, indicating a decrease in CYC proportion across the time course and in increase in ASC and NEU_A proportion between control and AstADs. E. Single cell average module gene expression of literature gene sets at 21 DIV3D highlighting the correlation with upregulated transcripts in human post-mortem AD datasets in NEU_A and reactive astrocyte markers and AD disease associated astrocyte markers in ASC (Source Table 1). (ns : p > 0.05, *: p <= 0.05, **: p<= 0.01, *** : p<=0.001). Inset box plots show the median, lower and upper hinges that correspond to the first quartile (25th percentile) and third quartile (75th percentile), and the upper and lower whiskers extend from the smallest and largest hinges at most 1.5 times the interquartile range. Dotted lines indicate median. F. Top 10 pathways from functional gene set enrichment of significant differentially expressed upregulated genes (see Methods, p <0.05, fold change > 0.25) between AstAD and control at each timepoint in NEU_A, NEU_B, and ASC presented as –log10 p-value. (Source Table 2). G. Single cell average module gene expression of ontology gene sets (Source Table 1) at 21 DIV3D highlighting the HSP, TNF inflammatory, positive regulation of neuron death, and transcriptional stress responses in NEU_A and ASC. (ns : p > 0.05, **: p<= 0.01, ****: p<= 0.0001). Inset box plots show the median, lower and upper hinges that correspond to the first quartile (25th percentile) and third quartile (75th percentile), and the upper and lower whiskers extend from the smallest and largest hinges at most 1.5 times the interquartile range. Dotted lines indicate median. H. Enrichment Map clustering presentation of functional enrichment results (see Methods, p < 0.01) with manual annotations across the 7 (light orange), 14 (orange), 21 DIV3D (dark orange) time course from significantly upregulated differentially expressed genes in NEU_A and ASC, identifying a range of upregulated responses to oTau induced pathology in AstAD.

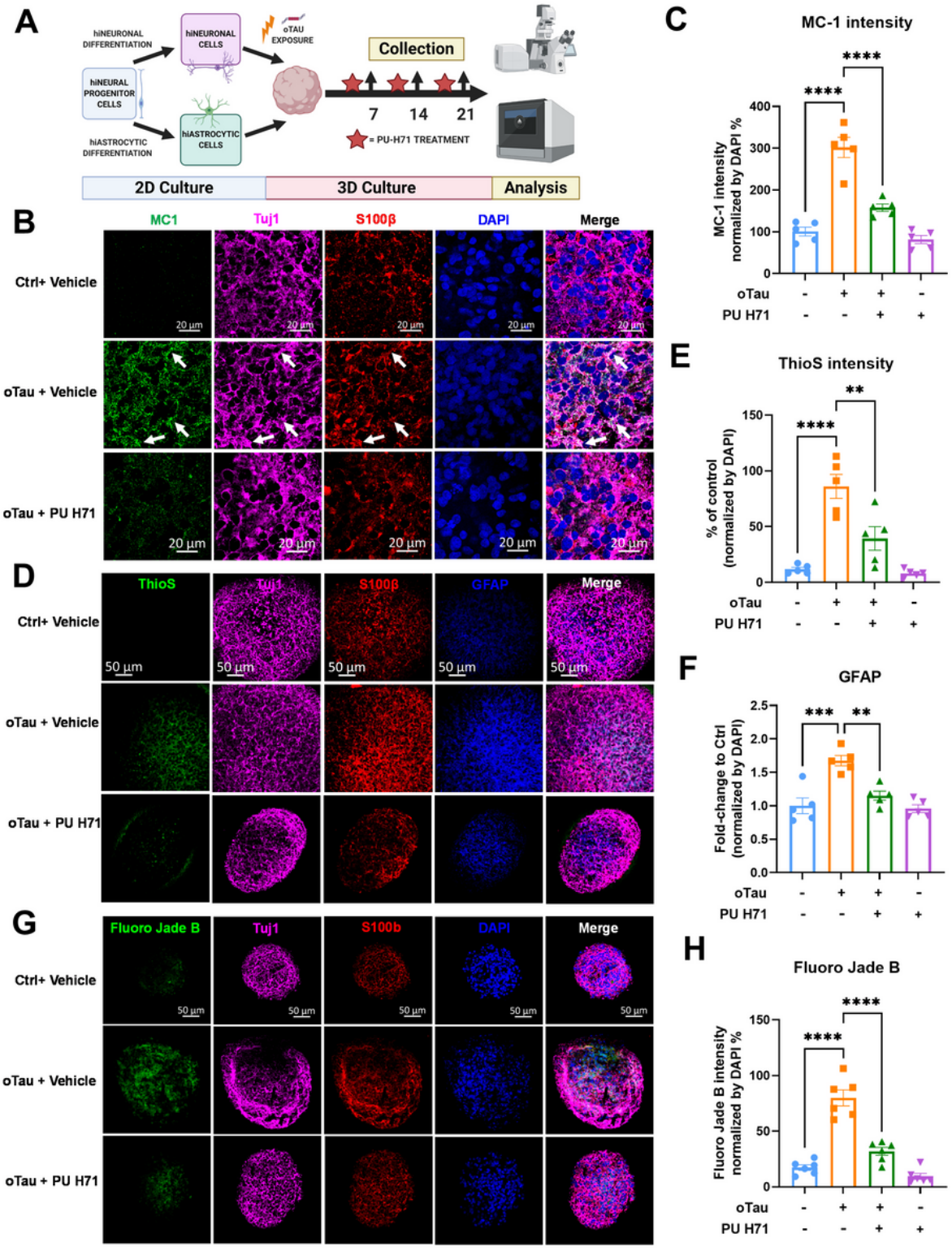

Figure 3

Epichaperome inhibitor PU-H71 treatment reduces oTau induced pathology and neurodegeneration. A. Experimental schematic including 2D culture, 3D culture, and analysis with indicated data collection harvest timepoints. B. Representative images showing reduction in tau misfolding in oTau seeded asteroids upon exposure to PU-H71 for 3 days, from days 19 - 21. The misfolded tau is labeled by MC1 (misfolded tau, green). Neurons were labeled by Tuj1 (βIII tubulin, violet) and astrocyte were labeled by

S100β (Red). Scale bars: 20 μm. C. Quantification of MC1 labeled fluorescence intensity normalized to the corresponding DAPI intensity. Data obtained from 5 independent asteroids. Error bars = SEM. One-way ANOVA with Tukey's multiple comparisons test was performed, ***p<0.001 comparisons to Vehicle control. D. Representative images showing reduction in ThioS, indicating fibrillar tau, in oTau seeded asteroids upon exposure to PU-H71 for 3 days, from days 19 - 21. The misfolded tau is labeled with MC1 (green). Neurons were labeled by Tuj1 (βIII tubulin, violet) and astrocyte were labeled with S100β (Red) and GFAP (Blue). Scale bars: 50 μm. E, F. Quantification of ThioS (E) and GFAP (E) labeled fluorescence intensity normalized to corresponding DAPI intensity. Data obtained from 5 independent asteroids. Error bars = SEM. One-way ANOVA with Tukey's multiple comparisons test was performed, ***p<0.001, **p<0.001 comparisons to Vehicle control. G. Representative images showing Neuro Jade B labeled fluorescence in oTau seeded asteroids upon exposure to PU-H71 for 3 days, from days 19 - 21. The damaged neurons are labeled by Neuro Jade B (green). Neurons were labeled with Tuj1 (βIII tubulin, violet) and astrocyte were labeled with S100β (Red) and GFAP (Blue). Scale bars: 50 μm. H. Quantification of Neuro Jade B labeled fluorescence intensity normalized to the corresponding DAPI intensity. Data obtained from 5 independent asteroids. Error bars = SEM. One-way ANOVA with Tukey's multiple comparisons test was performed, ***p<0.001 comparisons to Vehicle control.

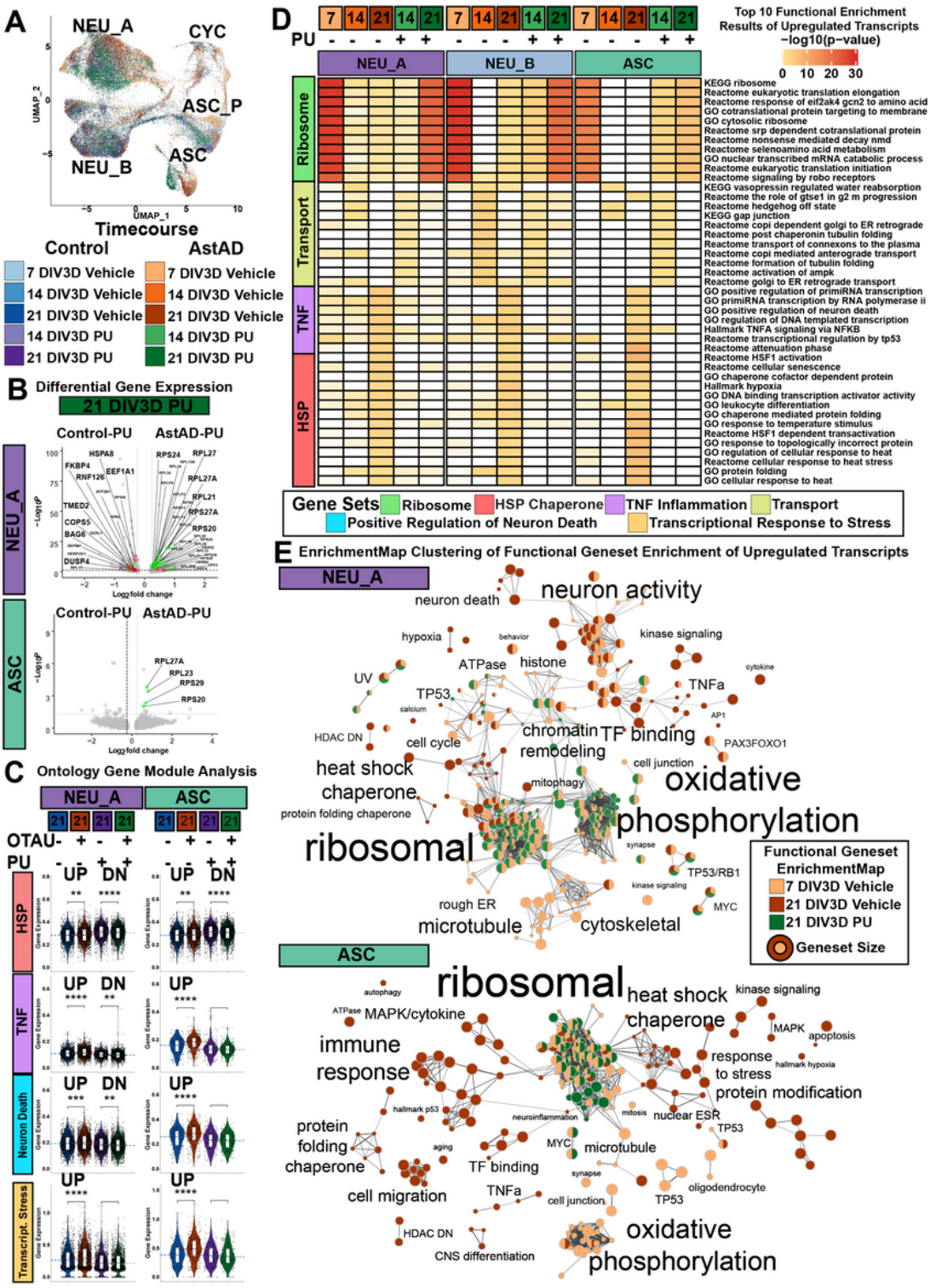

Figure 4

Single cell RNA-sequencing supports PU-H71 reversal of the pathological molecular phenotype. A. UMAP colored by experimental conditions across the 21 DIV3D control-vehicle, AstAD-vehicle, control-PU, and AstAD-PU time course (blue, orange, purple, and green gradients, respectively) highlighting model trajectory and cell typing with the addition of epichaperome inhibitor PU-H71. B. Differential gene expression between control and AstAD at 21 DIV3D-PU presented as volcano plots, demonstrating the

reversal of the 21 DIV3D-vehicle molecular phenotype to the 7 DIV3D-vehicle molecular phenotype with PU-H71 treatment. Dotted lines indicate the log 2 fold change significance of magnitude 0.25 and a p-value significance of 0.05. Significant differentially expressed ribosomal genes are highlighted in green, heat shock associated genes are highlighted in red, and TNF inflammatory genes are highlighted in purple. C. Single cell average module gene expression of ontology gene sets (Source Table 1) at 21 DIV3D- vehicle and 21DIV3D-PU highlighting the suppression of the HSP, TNF inflammatory, positive regulation of neuron death, and transcriptional stress responses with PU-H71 treatment. (ns: p > 0.05, **: p<= 0.01****: p<= 0.0001). Inset box plots show the median, lower and upper hinges that correspond to the first quartile (25th percentile) and third quartile (75th percentile), and the upper and lower whiskers extend from the smallest and largest hinges at most 1.5 times the interquartile range. Dotted lines indicate median. D. Top 10 pathways from functional gene set enrichment of significant differentially expressed upregulated genes (p <0.05, fold change > 0.25) between control and AstAD at each timepoint across in cell clusters NEU_A, NEU_B, and ASC presented as –log10 p-value with and without PU treatment. (Source Table 2). E. Enrichment Map clustering presentation of functional enrichment results (see Methods, p < 0.01) with manual annotations across the 7 DIV3D-vehicle (light orange), 21 DIV3D-vehicle (dark orange), and 21 DIV3D-PU (green) time course for significantly upregulated differentially expressed genes in NEU_A and ASC, identifying a range of upregulated responses in AstAD that are reversed with PU-H71 treatment.

Supplementary Files

This is a list of supplementary files associated with this preprint. Click to download.

- Video1A.CTR21DIV3Dlabel.mp4
- Video1B.oTAU21DIV3Dlabel.mp4
- asteroid1supplementalfigures21921.docx